Environmental Science & Technology

Article

pubs.acs.org/est

A Mobile Sensing Approach for Regional Surveillance of Fugitive Methane Emissions in Oil and Gas Production

John. D. Albertson,[*,†,§] Tierney Harvey,[§,▽] Greg Foderaro,[‡,○] Pingping Zhu,[‡] Xiaochi Zhou,[§] Silvia Ferrari,[‡,∥] M. Shahrooz Amin,[⊥,◆] Mark Modrak,[⊥,¶] Halley Brantley,[#] and Eben D. Thoma[#]

[†]School of Civil and Environmental Engineering and [‡]Sibley School of Mechanical and Aerospace Engineering, Cornell University, Ithaca, New York 14853, United States

[§]Department of Civil and Environmental Engineering and [∥]Department of Mechanical Engineering and Material Science, Duke University, Durham, North Carolina 27708, United States

[⊥]Arcadis-US Inc., 4915 Prospectus Drive F, Durham, North Carolina 27713, United States

[#]Office of Research and Development, National Risk Management Research Laboratory, United States Environmental Protection Agency, 109 TW Alexander Drive, E343-02, RTP, North Carolina 27711, United States

ABSTRACT: This paper addresses the need for surveillance of fugitive methane emissions over broad geographical regions. Most existing techniques suffer from being either extensive (but qualitative) or quantitative (but intensive with poor scalability). A total of two novel advancements are made here. First, a recursive Bayesian method is presented for probabilistically characterizing fugitive point-sources from mobile sensor data. This approach is made possible by a new cross-plume integrated dispersion formulation that overcomes much of the need for time-averaging concentration data. The method is tested here against a limited data set of controlled methane release and shown to perform well. We then present an information-theoretic approach to plan the paths of the sensor-equipped vehicle, where the path is chosen so as to maximize expected reduction in integrated target source rate uncertainty in the region, subject to given starting and ending positions and prevailing meteorological conditions. The information-driven sensor path planning algorithm is tested and shown to provide robust results across a wide range of conditions. An overall system concept is presented for optionally piggybacking of these techniques onto normal industry maintenance operations using sensor-equipped work trucks.

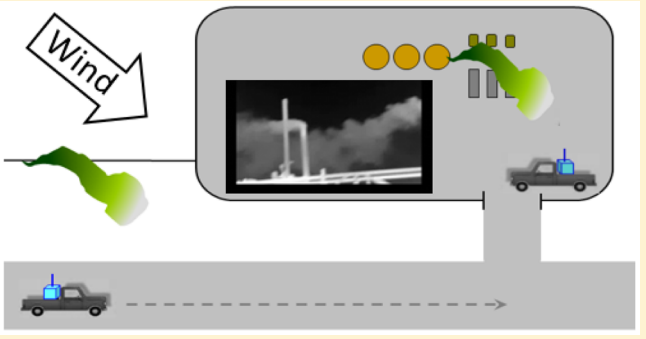

INTRODUCTION

Natural gas is considered to be one of the most attractive bridge solutions to carry the United States from its petroleum dependence to future renewable energy sources.[1] The attractive nature of gas stems from both the large domestic reserves of shale gas resources[2] and its potential lower greenhouse gas footprint vis-a-vis other fossil-fuel solutions.[3]

Recent advances in extraction technologies have led to a rapid increase in natural gas production rates,[4] which are expected to continue to increase over the coming decades.[5] There are currently about half a million natural gas production wells and one-third of a million miles of natural gas transmission pipelines in the United States.[5] Leaks at these well production and pipeline facilities release methane (CH_4) directly to the atmosphere, thus reducing the potential greenhouse forcing advantage over competing fossil fuels such as coal. Significant debate surrounds the aggregate magnitude of these fugitive emissions.[6] Much of the debate centers on whether the total losses are above or below the tipping point of 3.2%, beyond which natural gas is considered to be worse than coal from a greenhouse forcing perspective.[7]

The majority of efforts to characterize CH_4 emissions from oil and natural-gas production have focused on developing estimates of aggregate emissions, needed both to inform the national energy policy dialogue and to improve estimates of greenhouse forcing in climate forecasts. Good examples include the top-down approaches to estimate regional fluxes[8−10] and the intensive experimental investigations of individual sites[11−14] to support an estimate of emissions from representative types of facilities. Recent integrated research efforts have highlighted the importance of skewed emission distributions and the impact of high emitters on inventories.[15,16] Keying on the spatially distributed nature of natural gas production, mobile measurement approaches have been shown useful in identification of high-emitting facilities.[17−21] Zavala et al.[22] have recently defined functional superemitters (FSEs) as production sites with

Received: October 15, 2015
Revised: January 22, 2016
Accepted: January 25, 2016
Published: January 25, 2016

DOI: 10.1021/acs.est.5b05059
Environ. Sci. Technol. 2016, 50, 2487−2497

abnormally high emissions compared to their production capacity. Rapid identification and mitigation of malfunction-related FSE sites, as well as issues such as pipeline leaks, offer the potential for both reduced greenhouse-gas emissions and costs.

Most current mobile measurement approaches represent intensive field efforts and use specialized equipment and procedures for inverse source emission estimation. More routinely implementable forms of mobile CH_4 leak surveys have also been demonstrated,[23,24] but these surveys result primarily in the qualitative assessment of the roadway-measured concentrations rather than pinpointing locations and strengths of individual leaks as needed to target mitigation efforts. This paper helps move the mobile-measurement topic forward by describing a multilevel approach to identify and locate leaks and to quantify source rates using either dedicated mobile surveys or based in part on the concept of automated work-truck monitoring, in which methane sensors are mounted on vehicles traversing the region as part of ongoing operations.

Without the on-site release of tracer gases, the degree to which concentrations measured along a roadway can be used to inform estimates of point-source locations and emission rates depends strongly on local meteorological conditions. Given the complex nonstationary turbulent flows in the lower atmosphere, even the best source-inference models work well only under a restricted range of prevailing wind conditions,[25,26] with large errors under low wind speeds, shifting mean wind directions, strong convection, or stable inversions. Even approaches that use expensive precision instruments operated by trained personnel will periodically fail to meet accuracy targets, in addition to being prohibitively expensive for routine operation. There is a clear need for approaches that offer economic scaling to large numbers of sources over widespread regions. Both low- and high-cost sensors currently have very limited autonomy due to the lack of commercially available CH_4 sensor management and inference algorithms capable of integrating environmental conditions with turbulence models and heterogeneous sensor measurements.

This paper outlines a novel approach that is relevant for either the dedicated sensing of a region with optimal coverage scaling or for opportunistic regional sensing where CH_4 sensors are mounted on industry work trucks conducting routine activities in a region of interest. This is made possible because the sensing objectives are readily piggybacked on normal field and facility operations and maintenance efforts. For example, when trucks are parked at individual well pads, fugitive emissions can be assessed following the approach of Foster-Wittig et al.[26] This paper presents the technical basis for opportunistically assessing fugitive emissions from potential sources along travel paths of sensor-equipped vehicles under typical operational and maintenance efforts. The hierarchy of the proposed sensing philosophy is as follows:

1. Centralized controller: A remote cloud server is configured with a geospatial database of the location of all well pads in the region of interest and with the well ages and volume-flow rates of oil and gas. This server has real time access to meteorological forecasts (wind speed, direction, stability, etc.) and also to wind data from several micrometeorological sites located on larger well pads in the region. From this information, prior distributions of the probabilistic assessment of potential leak rates are given, and a simple estimate of dispersion or transport efficiency from each potential leak to each roadway segment can be calculated as needed to assess the relative sensing benefits of different travel paths from starting to destination well pads. An information-theoretic sensor-path-planning algorithm is employed to calculate optimal travel routes and to send navigation instructions to a vehicle-based dashboard display. The cloud server requirements would be easily met by a commercial provider or a single dedicated workstation housed remotely. The information needed to initialize the database is available from both industry-based sources and permitting documentation.
2. Sensor-equipped vehicles: methane sensors installed on either dedicated vehicles (for third party surveillance) or industry work trucks (for opportunistic sensing) collects data along its route, and these data are pushed to a cloud server where a Bayesian inference algorithm is employed to assign probabilistic leak-source distributions to the adjacent target wells. This step employs a cross-plume integrated turbulent dispersion model. These calculations are fully automated and based on the methods presented in this paper.
3. Leak mitigation: The database of emission estimates across the wells is updated recursively, and flags are triggered when leaks above a predetermined action level are identified to within an acceptable probability. This effort can easily be configured to subtract off any a priori acceptable emission levels at the wells, thus focusing on the "leak" aspect of the emissions.

This goal of this approach is to provide precision leak surveillance of targeted well pads, and opportunistic sensing of nontargeted well pads and pipelines along the work truck travel paths, providing further mitigation of health and safety risks at negligible added cost. This approach is made possible by a novel data analytics system, running on a private cloud server that performs both source inference and sensor-path planning.

TECHNICAL BACKGROUND

A method was developed to identify the location and strength of point-source fugitive emissions on well pads from a single sensor parked for a short recording period in the near- to midfield (some

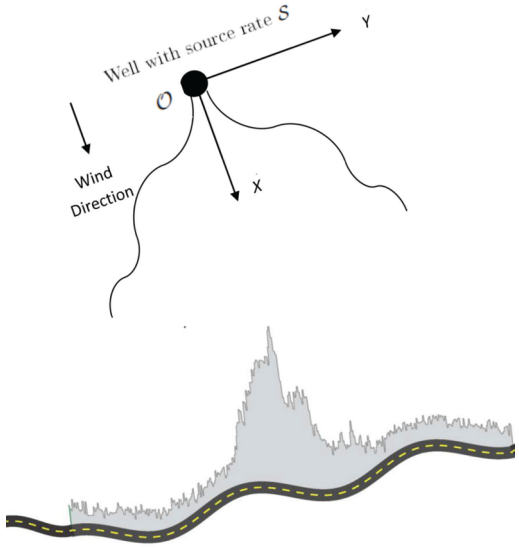

Figure 1. Local coordinate system and schematic of mobile plume measurements.

DOI: 10.1021/acs.est.5b05059
Environ. Sci. Technol. 2016, 50, 2487−2497

20 to 200 m downwind).[26] Such an approach is suitable for use with data from gas analyzers and anemometers mounted on either a dedicated sensor vehicle or an industry work truck parked for at least 20 min, collecting time-series data near a well pad during maintenance.

In this section we first present a method to characterize potential sources (at well pads or pipelines) located adjacent to a given travel route from one maintenance site to another. We refer to this as opportunistic mobile sensing, in which a sensor traverses a plume, providing a sort of cross-sectional view of its instantaneous form. We then present an information-theoretic approach to plan the paths of the work trucks between maintenance locations, where the path is chosen so as to maximize the expected reduction in integrated target source rate uncertainty in the region, subject to given starting and ending positions and prevailing meteorological conditions. If a dedicated sensing approach is desired instead, the same approach can be used to plan paths throughout a region that provide maximum information gain for distance traveled.

Source Inference from a Mobile Sensor. Here we focus on a single well pad (target) located along a traveled path. This target has an unknown methane source rate S. As shown in Figure 1, we adopt a local coordinate system $\mathcal{F} = (X, Y, Z)$ with origin O at the target and its X axis directed along the mean wind direction.

It is useful to describe the concentration C at the location (x, y, z) of a downwind sensor as

$$C(x, y, z) = \frac{S}{\overline{U}} D_y(x, y) D_z(x, z) \tag{1}$$

where S is the source strength at the origin, $\overline{U}$ is the effective speed of plume advection, and D_y and D_z are intended to account in a general way for the effects of lateral and vertical dispersion, respectively. At this early stage we are not making distinctions between instantaneous and ensemble-averaged quantities for reasons that will become clear later. However, for reference we can say that if we were to work in the limit of ensemble-averaged quantities, then D_y would be the oft-cited Gaussian shape function.[27−29] Moreover, it is important to note that we focus here on a single gas source contributing to $C(x, y, z)$, whereas in practice, the measured concentration can be a linear superposition of influences from multiple upwind sources. It is straightforward to implement an extension of these methods for multiple sources. However, for clarity in this subsection, we restrict the presentation to one source with a steady-state leak rate.

In the present application, with a mobile sensor traversing a plume, we are closer to an instantaneous concentration, and so D_y takes the form of a random function. However, in any case (e.g., instantaneous or longer time average), it is important to note that the cross-wind integral of D_y is unity; that is,

$$\int_{-\infty}^{\infty} D_y(x, y)\, \mathrm{d}y = 1 \tag{2}$$

This nicely removes much of the randomness when dealing with instantaneous plumes. This benefit is demonstrated when integrating (1) across the plume to relate the integrated concentration to the source rate of emissions

$$C^y(x, z) = \int_{-\infty}^{\infty} C(x, y)\, \mathrm{d}y = \frac{S}{\overline{U}} D_z(x, z) \tag{3}$$

where we write C^y for the cross-plume integrated concentration, and typically $D_z = \frac{A}{\overline{z}} \exp\left[-\left(\frac{Bz}{\overline{z}}\right)^s\right]$, where $\overline{z}$, s, A, and B are functions of atmospheric stability, and the average plume height $\overline{z}$ is also a function of x.[26,27] It is important to note that (3) is strictly applicable only in the case where the vehicle's path is *perpendicular* to the wind direction.

However, in field applications, the sensor path is typically limited to adjacent roadways, which are not always perpendicular to the wind direction. When the vehicle's path is at a significant angle to the wind direction, we propose a numerical integration of both sides of (1), such as

$$\begin{aligned} C^y &= \sum_{i=0}^{\infty} C(x_i, y_i) \Delta t V \\ &= S \sum_{i=0}^{\infty} \frac{\Delta t V}{\overline{U}_i} \left(\frac{A}{\overline{z}_i} \exp\left[-\left(\frac{Bz}{\overline{z}_i} \right)^s \right] \right) \left(\frac{1}{\sqrt{2\pi}\sigma_y} \right. \\ &\quad \left. \exp\left[-\frac{1}{2} \left(\frac{y_i}{\sigma_y} \right)^2 \right] \right) \end{aligned} \tag{4}$$

where i is a counter for the sensor position, Δt is the sensor recording time step, V is the vehicle speed, the traditional Gaussian shape function is used for D_y as a first approximation, σ_y is the horizontal length scale of the meandering plume, and y_i is the cross-wind distance from the plume center (as in Figure 1). In the case of a nonperpendicular sensor pass, both x and y vary across the plume (with i).[26,27]

As mentioned in the Introduction section, the prevailing meteorological conditions during a single sensor pass are rarely ideal for source inference. Nonetheless, non-negligible information can be gathered from each pass of a well target and used to partially reduce the uncertainty in fugitive emission rates. Therefore, we take a probabilistic view of fugitive emission rates and employ a recursive Bayesian inference, where the emission uncertainty can be updated after each sensor pass.

Following the Bayes rule, we can estimate the posterior probability density function (PDF) of the source rate S given the concentration data set $\mathcal{M}$ (i.e., the sensor data for a single plume traversal), ancillary information about the source W (e.g., well-pad age, complexity, and gas and oil production rate) and the prevailing meteorological conditions Λ (e.g., wind speed, direction, stability, and aerodynamic roughness):

$$p(S|\mathcal{M}, W, \Lambda) = \frac{p(S|W) p(\mathcal{M}|S, \Lambda)}{p(\mathcal{M}|\Lambda)} \tag{5}$$

where $p(S|\mathcal{M}, W, \Lambda)$ is the posterior distribution, $p(S|W)$ is the prior distribution, $p(\mathcal{M}|S, \Lambda)$ is the likelihood function, and the evidence $p(\mathcal{M}|\Lambda)$ simply ensures the posterior PDF integrates to unity.[30]

Prior to beginning sensing activities in a region of interest, we may have no specific information on the likely source rates of individual wells. However, from past measurements of oil- and gas-production well pads,[17] we do know that the source rates have a strong positive skew (e.g., the so-called fat tail) and follow reasonably well the Generalized Extreme Value Type II distribution. Therefore, we may adopt a prior distribution of

DOI: 10.1021/acs.est.5b05059
Environ. Sci. Technol. 2016, 50, 2487−2497

$$p(S|\mathcal{W}) = \frac{1}{\beta}\exp\left[-\left(1+\gamma\frac{(S-\mu)}{\beta}\right)^{-1/\gamma}\right]\left(1+\gamma\frac{S-\mu)}{\beta}\right)^{-1-1/\gamma} \quad (6)$$

where the parameters ($\gamma = 1$, $\mu = 0.19$, $\beta = 0.23$) have been estimated by a fit to the well-pad source emission estimates of Brantley et al.[17] Because it is widely held that source rates depend somewhat on the well-pad characteristics ($\mathcal{W}$), it would be a simple extension to specify the parameters in eq 6 to be functions of $\mathcal{W}$.

The recursive approach requires that the prior be set as

$$p(S|W)_j = \begin{cases} p(S|W) \text{ from (6)} & \text{for } j = 1 \\ p(S|\mathcal{M}, W, \Lambda)_{j-1} & \text{for } j > 1 \end{cases} \quad (7)$$

where j is a counter for successive passes of a single target.

The likelihood function describes how likely the data set $\mathcal{M}$ would be for a source rate of S and a prevailing set of meteorological conditions Λ. We adopt the traditional Gaussian likelihood function:

$$p(\mathcal{M}|S, \Lambda) = \frac{1}{\sigma_e\sqrt{2\pi}}\exp\left[-\frac{1}{2}\left(\frac{C^y - C^{y,M}(S)}{\sigma_e}\right)^2\right] \quad (8)$$

where $C^{y,M}(S)$ is the integral of a modeled concentration across y for a given assumed value of S, and σ_e is combined model and measurement error.[31] Note that with this likelihood function computed on a cross-plume integrated basis it is insensitive to mismatches in plume locations and widths that would occur due to meandering and the randomness of turbulent dispersion. We test this approach in the Results and Discussion section. However, before moving to that, we present below the technical foundation for the information-theoretic-based path planning for the navigation of the sensor vehicle(s). Note that we now transition from considering one well, with an unknown source rate, and a traversal of that single plume with the mobile sensor to considering an array of wells, all with unknown source rates.

Path Planning for Regional Coverage. The performance of a sensor is ultimately determined by how well the measurements it acquires satisfy its sensing objective. In the scenario considered, the mobile sensing vehicle must infer the value of hidden hypothesis variables, the unknown strengths of fugitive methane emissions, from remotely obtained concentration measurements and atmospheric data. Because the actual value of a particular measurement is unknown prior to obtaining it, this paper proposes a novel information-driven approach, based on expected information value, for the effective detection of fugitive emissions from oil and gas production sites. The objective of the methodology presented in this section is to determine an optimal path for the mobile sensing vehicle (e.g., industry work truck) between initial and final locations, such that the expected information gain of the sensor measurement is maximized while constraining the distance traveled. Because the path is to be determined before the measurements are known, the information gain is estimated using the expected entropy reduction (EER) method first proposed in ref 32.

Information entropy is simply a nonparametric measure of the uncertainty in a PDF. Thus, maximizing the entropy reduction is simply maximizing the reduction in the uncertainty (i.e., width) of a PDF. By extension, maximizing the EER over a path is analogous to minimizing the uncertainty in the overall set of source strength estimates obtained from the integrated sensor measurements.

Consider a region of interest (ROI) $\mathcal{W}$ that is populated by N wells, or other oil and gas production facilities, each of which represents a potential source of fugitive methane emissions with unknown source rate denoted by S_l, where $l = 1,..., N$. Because the source rate is unknown and cannot be observed, S_l is viewed as a continuous hidden random variable to be inferred from the set of concentration measurements, $\mathcal{M}$, and the set of meteorological conditions, Λ, based on the dispersion model in the previous section. Given cost and time constraints, it is impractical for the mobile sensing vehicle to simply obtain all possible measurements in $\mathcal{W}$. Therefore, an optimal sensing path is one that enables the measurement sequence with the maximum information gain for the hypothesis variable(s), S_l, while placing practical constraints on total distance traveled.

Thus, let the continuous random variable $M_{l,k}$ represent an integration of the concentration measurements across the plume from the lth well on the kth road segment (e.g., LHS of eq 4). Then, to determine the optimal path, the expected value of the information gain of the future measurement $M_{l,k}$ must be estimated a priori using the expected reduction in integrated source uncertainty over any road segment, as described in the next section.

Information Value Function. Information theoretic functions have been proposed for the purpose of assessing the expected information gain of future sensor measurements.[32−34] These functions are implemented in sensor management problems to optimize sensor performance by determining the expected information value of future sensor measurements. In particular, information entropy can be used to determine the uncertainty in a continuous random variable R based on its PDF, $p(R)$.[35] Zhang et al.[34] found that information-driven search strategies based on quadratic entropy typically outperform alternate information functions, such as the α-divergence and Cauchy-Schwarz distance, in the classification of hypothesis variables. The quadratic entropy, also known as Rény entropy of order $\alpha = 2$, is defined as

$$H(R) = \frac{1}{1-\alpha}\log_2\int_{r\in\mathcal{R}} p^\alpha(r)dr \quad (9)$$

where $r \in \mathcal{R}$ denotes a value in the random variable range $\mathcal{R}$. Subsequently, for a process with three interrelated random variables P, Q, and R, the reduction in uncertainty brought about by Q when R is given can be represented by the change in conditional entropy or conditional mutual information,

$$I(P;\, Q|R) = H(P|R) - H(P|Q, R) \quad (10)$$

where $H(P|Q)$ denotes the conditional entropy of P given Q.[35]

It follows that if a data set $M_{l,k}$ were available, then the conditional mutual information $I(S_l;\, \mathcal{M}_{l,k}|\Lambda, W)$ could be used to represent the reduction in the uncertainty in the source rate S_l, for given meteorological and ancillary source information, Λ and W. However, because the mobile vehicle path is to be computed prior to obtaining the measurements, the conditional mutual information in eq 10 cannot be used directly for sensor path planning, but the information gain from future measurements along any road segment (k) can be approximated using the EER, defined as

DOI: 10.1021/acs.est.5b05059
Environ. Sci. Technol. 2016, 50, 2487−2497

$$\varphi_{l,k}[S_l;\ \mathcal{M}_{l,k}|\Lambda,\ W] = \mathbb{E}_{\mathcal{M}_{l,k}}\{I(S_l;\ \mathcal{M}_{l,k}|\Lambda,\ W\} = H(S_l|\Lambda,\ W) - \mathbb{E}_{\mathcal{M}_{l,k}}\{H(S_l|\mathcal{M}_{l,k},\ \Lambda,\ W)\} = H(S_l|\Lambda,\ W) - \int_{m\in\mathcal{M}} H(S_l|M_{l,k} = m,\ \Lambda,\ W) \times p(M_{l,k} = m|\Lambda,\ W)\mathrm{d}m \quad (11)$$

where $\mathbb{E}_{\mathcal{M}_{l,k}}$ denotes the expectation with respect to the measurements $\mathcal{M}_{l,k}$, and $H(\cdot)$ is the quadratic entropy defined in eq 9. The information function above defines the expected reduction in uncertainty of the source strength S_l from the possible measurement $\mathcal{M}_{l,k}$, given Λ and W.

The first term in eq 13 is the prior entropy, which can be calculated by the prior distribution $p(S_l|\Lambda, W)$. Next, we discuss the calculation of the second term, the estimate of the posterior entropy, $\mathbb{E}_{\mathcal{M}_{l,k}}\{H(S_l|\mathcal{M}_{l,k}, \Lambda, W)\}$. Then, given Λ and W, the posterior distribution can be obtained by

$$p(S_l|M_{l,k} = m,\ \Lambda,\ W) = \frac{p(M_{l,k} = m|S_l,\ \Lambda,\ W)p(S_l|\Lambda,\ W)}{p(M_{l,k} = m|\Lambda,\ W)} = \frac{p(M_{l,k} = m|S_l,\ \Lambda,\ W)p(S_l|\Lambda,\ W)}{\int_{s\in\mathcal{S}} p(M_{l,k} = m|S_l = s,\ \Lambda,\ W)p(S_l|\Lambda,\ W)} \quad (12)$$

The prior distribution of the source strength $p(S_l|\Lambda, W)$ is initialized using (6). The conditional PDF $p(M_k = m_k|S_l, \Lambda, W)$, also known as the Likelihood function, is computed from

$$p(M_{l,k} = m|S_l = s,\ \Lambda,\ W) = \frac{1}{\sigma_e\sqrt{2\pi}}\exp\left[-\frac{1}{2}\left(\frac{m - C^{y,M}(S_l = s,\ \mathbf{x},\ \Lambda)}{\sigma_e}\right)^2\right] \quad (13)$$

where σ_e is the combined model and measurement error, and $C^{y,M}(S_i = s,\ \mathbf{x},\ \Lambda)$ is the cross-plume integrated concentration computed from a Gaussian dispersion model using the source strength $S_l = s$, the meteorological conditions Λ, and the position of the sensor $\mathbf{x}$.

The EER of a particular measurement sequence can then be calculated using eq 13 and used in a decision tree to determine the optimal sensing strategy for the mobile sensing vehicle.

Decision Tree. This subsection presents a methodology for determining an optimal sensing path for the mobile sampling vehicle between given initial and final positions $\mathbf{x}^0$ and $\mathbf{x}^F$, respectively, such that the expected information profit of the sensor task is maximized. The planning problem is represented by a decision tree, which is used to compute the optimal sensing strategy (σ^*). In the context of the sensing problem considered here, a strategy refers to the sequence of road segments traversed by the sensor that form a path in $\mathcal{W}$ and the associated measurement decisions. The optimal path for the sensor results in concentration measurements that provide the lowest expected posterior uncertainty in source-strength estimates.

The mobile sensing vehicle is restricted to the system of paved and dirt roads in the ROI. This road network can be represented compactly by a nondirected connectivity graph,[36] which is defined as follows.

Definition 1. A connectivity graph $\mathcal{G}$ is a nondirected graph, where nodes represent road intersections, and two nodes κ_ξ and κ_η in $\mathcal{G}$ are connected by an arc $(\kappa_\xi, \kappa_\eta)$ if these two corresponding intersections are connected by a road segment.

Let $\kappa_0 = \kappa[\mathbf{x}^0]$ and $\kappa_F = \kappa[\mathbf{x}^F]$ denote the initial and final intersections, respectively, of the mobile sensor. All of the admissible paths for the sensor between κ_0 and κ_F can be represented by a connectivity tree.

Definition 2. A connectivity tree $\mathcal{T}$, associated with $\mathcal{G}$, is an acyclic tree graph with root κ_0 and κ_F in the leaves.[33] Each branch of $\mathcal{T}$ corresponds to a unique sequence of roads and intersections that can be followed by the mobile sampling vehicle when traveling from κ_0 to κ_F.

A decision tree, represented by the tuple DT = $\{C, \mathcal{D}, J, \mathcal{A}\}$, is an acyclic graph with a treelike structure that is used to describe a discrete time-decision process, where C is the set of chance nodes, $\mathcal{D}$ is the set of decision nodes, J is the optimization cost function, and $\mathcal{A}$ is the set of directed arcs.[37] Decision nodes represent decision variables, chance nodes represent hypothesis variables, and utility nodes or leaves represent the value of the cost function. The decision tree is constructed using the following assignments:[32]

1. The root is κ_0, and every node preceding a utility node is κ_F.
2. Every chance node $\kappa_\xi \in C$ represents an intersection in $\mathcal{G}$.
3. An arc $(\kappa_\xi, \kappa_\eta) \in \mathcal{A}$ represents the decision to move from intersection κ_ξ to κ_η along the road associated with a reward R.
4. The utility node at the end of each branch represents the cumulative expected entropy reduction of the corresponding strategy.

As discussed in the Information Value Function section, the expected information profit with respect to the source strengths given a measurement sequence $\mathcal{M}_\tau$ is given by the expected entropy reduction. Then, for each arc, the EER of a measurement sequence $\mathcal{M}_k$ that would be obtained on the road segment, τ, is

$$R_k = \sum_{l=1}^{N_k} \varphi[S_l;\ \mathcal{M}_{l,k}|\Lambda,\ W] \quad (14)$$

where k indicates the index of the road segment in a path, and $N_k \leq N$ denotes the number of the wells whose plumes overlay road segment k.

Then, the optimal sensing strategy corresponds to the path of maximum cumulative entropy reduction of the source strength estimates. For a strategy σ_m, the cumulative EER is given by

$$E_c = \sum_{k=1}^{K} R_k \quad (15)$$

where K is the number of the arcs on a path. To constrain the selected path to a reasonable practical length, we add a penalty of path distance to the cost function. The following modified ratio between EER and path distance is designed as the cost function,

$$J = \frac{E_c}{1 + \zeta\ \exp(d - \lambda d_{\min})} \quad (16)$$

where d and $d_{\min}$ denote the path distance and the minimum distance of the possible paths, respectively.

In addition, ζ and λ are user-design parameters, which are applied to vary the penalty of the path distance. In this paper, these parameters are set to $\zeta = 0.8$ and $\lambda = 1.5$.

Finally, the optimal strategy σ^* can then be found from,

DOI: 10.1021/acs.est.5b05059
Environ. Sci. Technol. 2016, 50, 2487−2497

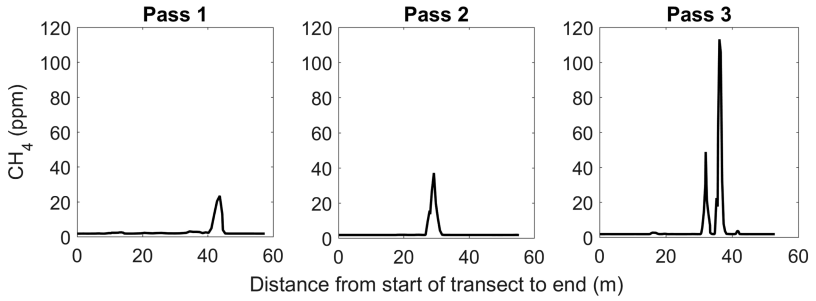

Figure 2. The measured CH_4 concentration from the instantaneous plume seen by the single-mobile sensor. The horizontal axis shows the distance traveled by the vehicle from the start of the transect to the end. These measurements were all made from the same controlled-release setup with three different passes downwind of the source.

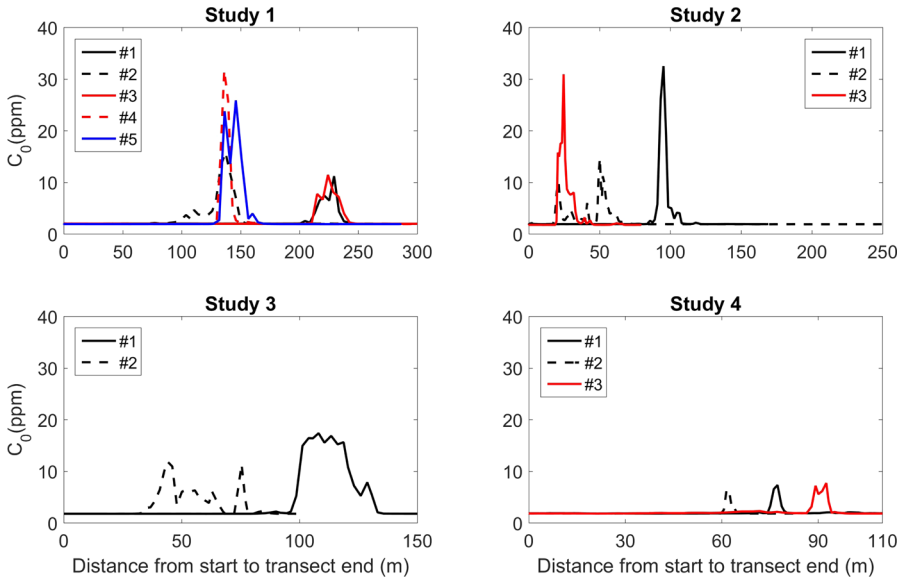

Figure 3. Measured plume concentration along the distance of the road for all four of the field data files.

$$\sigma^* = \arg\max_{\sigma_m}\{J[\sigma_m]\} \tag{17}$$

The methodology presented here utilizes a decision tree to determine σ^*.

Algorithmic Approach. For clarity, the path-planning approach is implemented as

1. Build connectivity graph; $\mathcal{G}$
2. Build connectivity tree with initial position at root and goal position in leaves;
3. Initialize priors using GEV;
4. Compute along each branch the cumulative EER of following a hypothetical measurement sequence;
5. Select the branch with the maximum cumulative EER;
6. Branch corresponds to a measurement strategy (i.e., path);
7. Perform measurements;
8. Update posteriors; and
9. Return to step 4 when planning the next path for the sensor.

EXPERIMENTAL DATA

The proposed method uses data acquired by single-sampling-point mobile approaches that utilize a relatively high-frequency (≥1 Hz) concentration measurement instrument (CMI) and stationary meteorological measurements, similar to that generally describe in EPA method OTM33A,[25] and is typically applicable near ground sources approximately 20 to 200 m downwind of the potential source. The trial mobile data described here used a sport utility vehicle equipped with a Picarro G1301-fc (Sunnyvale, CA) CMI, a model 81000 V three-dimensional (3D) sonic anemometer (R.M. Young, Traverse City, Michigan), and a high-performance global positioning system (GPS) (Hemisphere GPS, Calgary, Alberta, Canada). Using a mobile OTM 33 collection approach, data were collected for both a controlled release (CR) experiment and field studies. The controlled release experiment was conducted on May 15, 2010 in Durham, North Carolina, where three passes were made for the one CR experiment (Figure 2). The point-source release rate was controlled at $S = 0.6$ g/s. The plume position changes over time with the meandering wind, as shown in Figure 2.

Additionally, four field studies were conducted in Colorado on four separate days in July 2010, with the number of passes for each study ranging from two to five (Figure 3). We purposely chose regions with flat terrain to minimize the effects of topography, such that the existing published form for D_z should apply. For each location, after identifying the presence of a localized point source plume, the sensor vehicle was parked in a nearby open area to collect useful data on the mean meteorological conditions (e.g., 20 min of data). Then, the sensor vehicle traversed the plume of elevated CH_4 concentrations multiple times. Finally, the vehicle was parked for another 20 min to obtained additional meteorological data. The

DOI: 10.1021/acs.est.5b05059
Environ. Sci. Technol. 2016, 50, 2487−2497

meteorological data collected before and after the passes are used to estimate the mean wind speed, friction velocity, and stability parameter for use in the dispersion model detailed above.

Figure 3 shows the measured CH_4 concentration (C_o) collected during the field experiments in Colorado. The concentration shown is the measured concentration C_o; however, for analysis we use the measured concentration above background:

$$C = C_o - C_b \tag{18}$$

where C_b is the background concentration, taken from measurements outside the plume. For a robust estimate, C_b is calculated as the fifth percentile of the ranked C_o.

RESULTS

In this section we first examine the skill of the recursive Bayesian inference for fugitive point source emissions from a mobile sensor and then we explore the utility of the information-theoretic-based path planning algorithm.

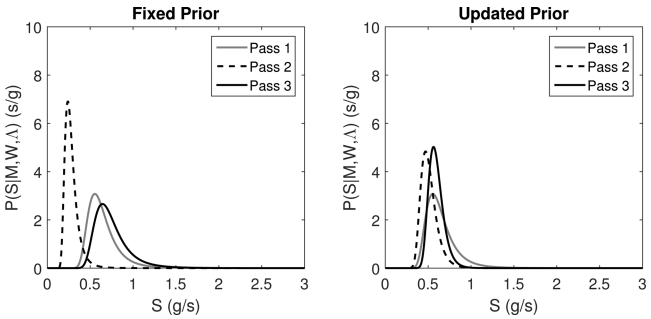

Figure 4. Left: posterior-source PDFs of the three controlled release passes using a fixed prior distribution. Right: posterior PDFs of the three passes using an updated prior distribution.

Table 1. Controlled Release Results[a]

pass	z_s (m)	S_o (g/s)	$S_{B,F}$ (g/s)	$S_{B,U}$(g/s)
1	1.5	0.6 ± 0.03	0.65	0.65
2	1.5	0.6 ± 0.03	0.27	0.51
3	1.5	0.6 ± 0.03	0.73	0.60

[a] z_s is the source height, S_o is the known release rate for the controlled releases, and $S_{B,F}$ is the inferred release rates with fixed prior, and $S_{B,U}$ with the recursively updated prior.

Source Inference from a Mobile Sensor. As discussed in the section of source inference using mobile sensor, the integration of the concentration across the plume removes much of the randomness from the dispersion effects and is intended to improve source inference skill. Here, we test this approach against the controlled point source release experimental data described in the Experimental Data section.

We first examine the model performance with controlled release experiments. Meteorological parameters, such as the Obukhov length (L) and friction velocity (u^*), are derived from data collected by a nearby, stationary three-dimensional (3D) sonic anemometer. Due to the short amount of time for a complete pass (around 2 min), we used the same meteorological values for all passes within a study. To explore the recursive aspect of the Bayesian inference using data from multiple passes, we compare the recursive posterior PDF (7) to an approach that computes the posterior PDF independently for each pass using the original GEV prior (6) and then averages these resulting

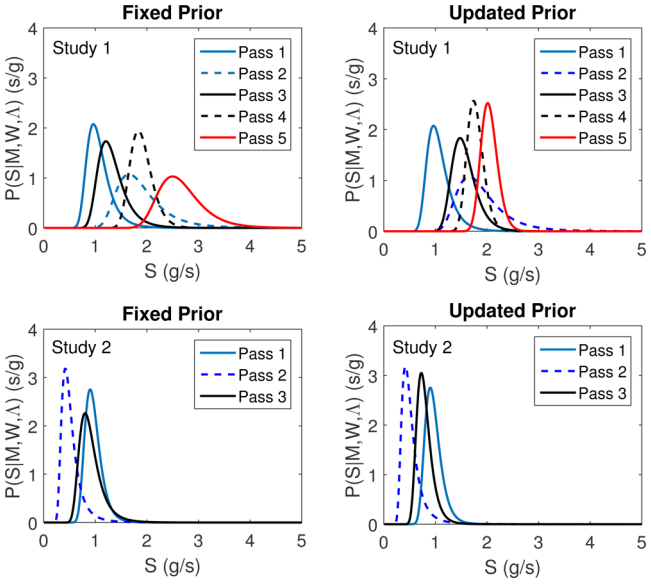

Figure 5. Posterior-source PDFs for Study 1 passes 1 to 5 (top) and Study 2 passes 1 to 3 (bottom) with fixed prior (left) and updated prior (right).

Table 2. Field Study Results[a]

study	passes (#)	z_s (m)	$\overline{S_{B,F}}$ (g/s)	$S_{B,U}$ (g/s)
1	5	3	1.8	2.1
2	3	3	0.8	0.8
3	2	3	1.6	1.4
4	3	3	0.18	0.16

[a] z_s is the estimated source height, $\overline{S_{B,F}}$ is the average of the expected values of the source strength from the individual passes using Bayesian inference with a fixed prior, and $S_{B,U}$ is the result of the final pass using Bayesian inference with a recursively updated prior.

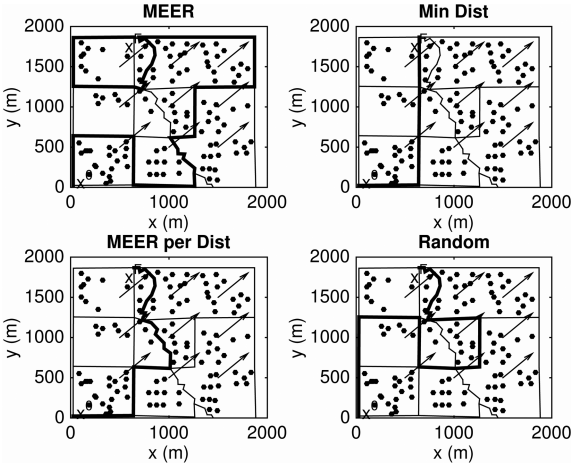

Figure 6. Paths from the initial position x^0 to the final position x^F, where the black dots represent the wells, and the arrows represent the wind directions.

posterior PDFs. These posterior PDFs for each pass (no averaging yet) are shown in Figure 4. It is encouraging that the posterior source PDFs for both approaches peak around the true release rates of 0.6 g/s, except for pass 2 with the fixed posterior, which shows significant underestimation. In comparing these two approaches, it appears that the recursive updating leads to more accurate leak rate estimation and reduced uncertainty (a

DOI: 10.1021/acs.est.5b05059
Environ. Sci. Technol. 2016, 50, 2487−2497

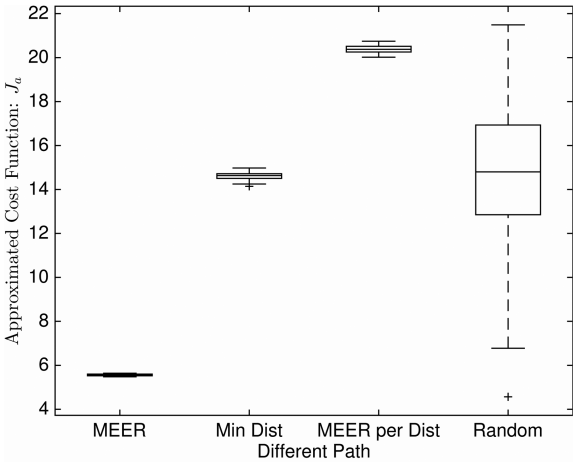

Figure 7. Approximated cost function values (J_a) for different paths of Figure 6, where the central mark is the median, the edges of the box are the 25th and 75th percentiles, and the whiskers extend to the most extreme data points.

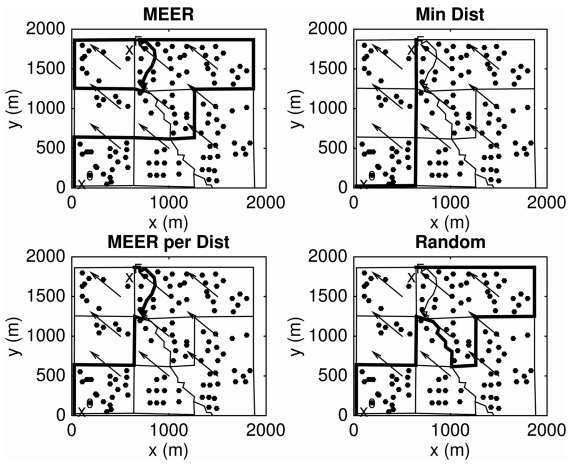

Figure 8. Paths from the initial position x^0 to the final position x^F, where the black dots represent the wells, and the arrows represent the wind directions.

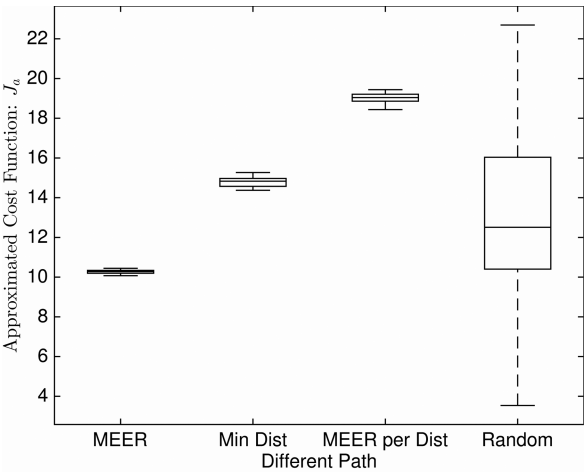

Figure 9. Approximated cost function values (J_a) for different paths of Figure 8, where the central mark is the median, the edges of the box are the 25th and 75th percentiles, and the whiskers extend to the most extreme data points.

sharpening of the estimate) with an increased number of sensor passes.

The expected values of these posterior source PDFs are computed by

$$S = \int_{S_{min}}^{S_{max}} p(S|\mathcal{M}, W, \Lambda) S \, dS \tag{19}$$

We present these source estimates in Table 1, using $S_{B,U}$ for the estimate using eq 19 applied to the recursive derived posterior (i.e., subscript U for "updated prior") and $S_{B,F}$ for the independent Bayesian inference using a fixed prior (i.e., subscript F for "fixed prior"). However, as stated above, the recursive approach offers a marked reduction in the uncertainty of the estimate. These results are encouraging for mobile sensing of fugitive methane emissions.

The recursive Bayesian approach converged precisely to the controlled release rate of 0.6 (g/s), whereas the average across the three fixed prior estimates is 0.55 (g/s). This cross-wind integrated plume approach seems promising and will become the subject of future extensive testing.

With some confidence in the source inference using mobile sensor given controlled releases, we move to examine data from field measurements in oil and gas production regions (non-controlled releases). These data are representative of the normal field conditions under which we propose this method for opportunistic sensing of targets along roadways during normal operation of industry work trucks. In Figure 5, we present results for two different locations, one with five passes and the other with three passes. The true release rates are not known in these cases. We continue the comparison of the recursive approach to the independent Bayesian with constant priors, showing the reduced uncertainty benefit of the recursive approach. The expected value of the source estimates from eq 19 are presented for all four studies along with ancillary data in Table 2. These results suggest that the approach provides promising results in both controlled and real-field conditions. This motivates the need to plan the path of these mobile mounted sensors to provide a means to sense wide arrays of targets in a region, making use of knowledge of the wind direction and the previous sensing data and the resulting estimates of source uncertainty.

Regional Path Planning. We focus this demonstration on an oil and gas production region outside of Greeley, CO (40°13′32.68″ N, 104°42′23.47″ W). We are using this geographical area as an example to explore the utility of the path planning algorithm. It is important to note at the outset that this section of the paper is based completely on simulations; no actual field data are used below other than the geographical setting.

In planning a set of measurements, there can be an absence of local data on the emission rates, and hence we assume at the outset an a prior probability of emissions from each well pad that follows the GEV distribution of eq 6 as fit to well-pad emission rates from other studies. A planned path, in the context of the proposed method, is defined on the basis of a given starting location ($\mathbf{x}^0$) and a given destination ($\mathbf{x}^F$) and is computed so as to maximize the objective function under the prevailing meteorological conditions. To demonstrate both the utility of the approach and its robustness to different start−end positions and wind directions, we explore results for three different pairs of start−end positions, and for each pair we consider four different wind directions. For each of these 12 cases, we plan a path that maximizes our objective function (expected entropy reduction, adjusted to constrain the route distance) and compare the

DOI: 10.1021/acs.est.5b05059
Environ. Sci. Technol. 2016, 50, 2487−2497

Table 3. Approximated Cost Function J_a[a]

start → end (X,Y) [km]	MEER	minimum Dist	MEER per Dist	random
		wind direction: 0		
(0,0) → (0.6,1.9)	15.84 ± 0.17	20.70 ± 0.26	27.18 ± 0.28	11.48 ± 5.39
(0,0) → (1.9,1.9)	36.26 ± 0.24	30.65 ± 0.37	36.34 ± 0.26	16.58 ± 5.27
(0,0) → (1.4,0)	17.66 ± 0.15	4.25 ± 0.14	19.91 ± 0.25	6.12 ± 3.45
		wind direction: $\pi/4$		
(0,0) → (0.6,1.9)	5.56 ± 0.04	14.61 ± 0.19	20.40 ± 0.17	14.31 ± 3.70
(0,0) → (1.9,1.9)	10.69 ± 0.10	21.17 ± 0.25	34.75 ± 0.27	22.22 ± 5.69
(0,0) → (1.4,0)	4.98 ± 0.05	0 ± 0	16.90 ± 0.28	8.00 ± 3.65
		wind direction: $\pi/2$		
(0,0) → (0.6,1.9)	5.04 ± 0.05	0 ± 0	20.06 ± 0.29	14.36 ± 5.60
(0,0) → (1.9,1.9)	33.38 ± 0.37	2.31 ± 0.13	40.05 ± 0.54	25.06 ± 9.71
(0,0) → (1.4,0)	5.40 ± 0.06	0 ± 0	11.95 ± 0.18	6.00 ± 3.01
		wind direction: $3/4\pi$		
(0,0) → (0.6,1.9)	10.28 ± 0.09	14.79 ± 0.22	19.02 ± 0.24	13.15 ± 4.36
(0,0) → (1.9,1.9)	24.79 ± 0.15	5.18 ± 0.15	38.31 ± 0.26	21.31 ± 6.78
(0,0) → (1.4,0)	2.87 ± 0.02	1.59 ± 0.14	12.51 ± 0.09	7.52 ± 3.16

[a]The results in these tables are in the form of mean ± standard deviation.

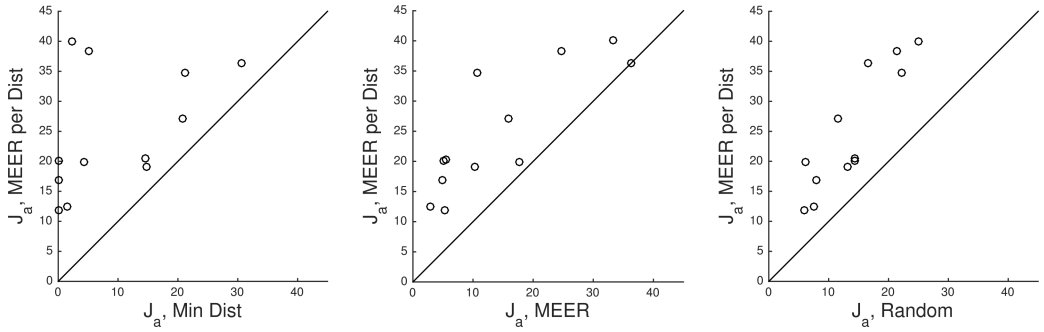

Figure 10. Approximated (actual) cost function (J_a) from the suggested "optimal" path (MEER per Dist) compared to the three alternative routes.

posterior utility of this path with three other path options that represent: (1) maximum EER (with no penalty for distance), (2) minimum distance, and (3) a randomly chosen route.

For illustration, we begin by considering a case where a sensor-equipped work truck has just completed maintenance activity at a well pad near the bottom left of the area in Figure 6 and has been assigned a destination located on the northern border of the domain, marked $\mathbf{x}^F$. The wind direction, in this case, is from the SW and is denoted by an array of arrows. The top right panel shows the minimum distance path, which does not take any sensing objectives into account. The bottom right panel shows a longer but random path. The top left panel is the path with the maximum total EER, following an approach much as proposed herein, except without the denominator term in J that serves as a distance penalty. The optimal path, based on the proposed approach, is shown in the bottom left panel.

We test the performance of the path-planning method by sampling simulated concentration data along the alternate paths, where the methane concentrations are generated by a simple 2D Gaussian plume dispersion model with source locations at each of the well pads noted in Figure 6. The sampled concentrations are used in eq 5 to estimate the posterior distributions. The actual entropy reduction from the prior to the posterior is computed and summed along the route and normalized by the adjusted travel distance as in eq 16. Following a Monte Carlo framework, this is conducted for 50 different realizations in each case, thus avoiding spurious results in which one path has a strong entropy reduction only because a strong leak rate was assigned to a well located just upwind of one road segment. The merits of the different routes for the case of Figure 6 are compared in Figure 7, where the approximated cost function (J_a) is simply J computed with the "actual" entropy reduction rather than the "expected" entropy reduction. The proposed route (MEER per Dist) is shown to offer robustly superior performance across the 50 realizations. For each realization, we randomly select a route to compare with our proposed algorithm. This ensures that the proposed route is compared broadly to other possible routes and it explains why the random route has the broader range of J_a values. In addition, one realization of a random route is shown in Figure 6 and 8.

We now move to consider a different wind direction (from the southeast) for the same start and end locations. Note the difference in the "optimal route" (i.e., MEER per Dist) shown in Figure 8 as compared to Figure 6, which is due to the obvious added merit to be downwind of uncertain sources. This is automatically taken into account in the path planning algorithm. As shown in Figure 9, the proposed route is also clearly superior to the considered alternatives.

Table 3 reports the results across all 12 of the different cases (three start−end location pairs by four wind directions each). The coordinates in X and Y of the start and end points are presented in the Table 3. The J_a values across the 50 realizations in each case are reported by the mean ± the standard deviation. We note that the superiority of the MEER per Dist approach is robust with respect to different wind directions and start-end locations. This is further depicted in the scatter plot of Figure 10,

DOI: 10.1021/acs.est.5b05059
Environ. Sci. Technol. 2016, 50, 2487−2497

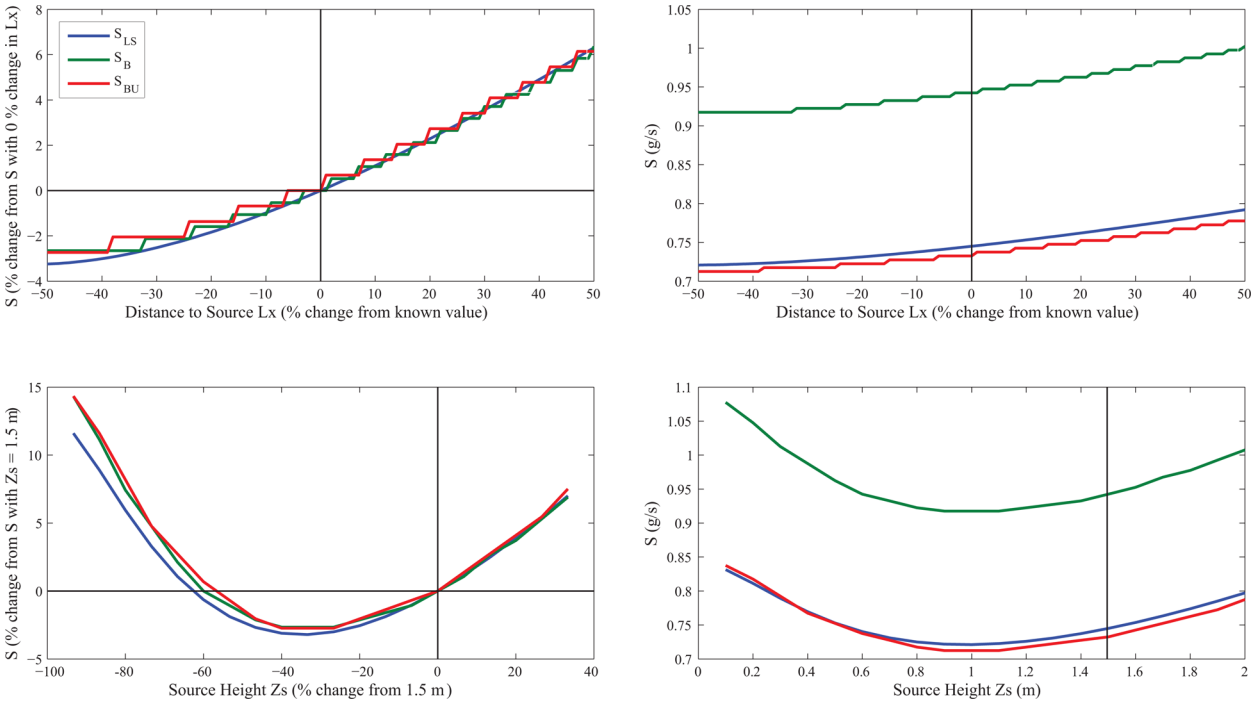

Figure 11. Sensitivity results for the CR release files with sensitivity to distance from the source L_x (top) and source height Z_s (bottom).

where the MEER per Dist route is shown to have greater entropy reduction than the other three approaches, for all 12 of the cases.

DISCUSSION

Methane emissions from oil and gas production regions is a topic of considerable contemporary interest. Existing approaches do not scale well economically. The approach presented in this paper is applicable to either dedicated regional surveillance or to an approach where the sensing objectives are piggy-backed onto normal industry maintenance activities in a region of interest. This opportunistic sensing approach provides repeated observations, which are especially important given the negative impact of many meteorological conditions (e.g., stable stratification, low wind speeds, etc.) on source inference. The proposed Bayesian approach provides a rigorous probabilistic assessment of the fugitive source emission rates, which allows for recursive refinement of the estimate until an acceptable confidence level is reached for triggering mitigation action.

The cross-plume integrated approach derived and presented here was shown to alleviate much of the difficulty inherent in instantaneous concentration measurements and provides highly accurate estimates of the point-source leak rates. With this approach validated on controlled release data and demonstrated in field conditions, we then explored how it can be scaled to the region with an information-theoretic sensor path planning approach. The path planning work was demonstrated here using simulated wind and concentration fields. However, given the promising results, it will be used in future field efforts and further explored in subsequent publications.

An interesting question is how well this approach will work if there is uncertainty about the precise location of a leak on a target well pad. In particular, there may be uncertainty in the height of the source and the upwind distance to the source. We examine in Figure 11 the sensitivity of the source rate inference to these two variables. It is encouraging that a 10% error in source height has a <3% impact on *S*. Similarly, the inferred value of *S* is not very sensitive to the assigned longitudinal distance from the source, with a 50% error in longitudinal distance impacting S by no more than 6%.

With the basic framework presented and demonstrated here for assessing single sources in open, relatively flat terrain, future work will be focused on modifications to the vertical dispersion formulation for complex topographies and the development of techniques for discriminating between multiple adjacent sources at different heights.

AUTHOR INFORMATION

Corresponding Author

*Phone: +1 (607)255-9671; fax: +1 (607)255-9004; e-mail: albertson@cornell.edu.

Present Addresses

[∇]Department of Engineering and Physics, University of Central Oklahoma, Edmond, OK, 73034, United States

[○]Applied Research Associates Inc., 8537 Six Forks Rd, Raleigh, NC, 27615, United States

[◆]NIMA Group LLC, 4700 Rochester Road, Troy, MI, 48085, United States

[¶]Aecom Technology Corporation, 9400 Amberglen Boulevard, Austin, TX, 78729, United States

Notes

The authors declare no competing financial interest.

ACKNOWLEDGMENTS

This work was supported by the NSF IGERT through Grant DGE-1068871 and U.S. EPA ORDs Air, Climate, and Energy (ACE) program. The authors thank Bill Squire and Bill Mitchell from EPA for their efforts on this project. The views expressed in this article are those of the authors and do not necessarily represent the views or policies of the U.S. Environmental Protection Agency. Mention of trade names or commercial products does not constitute endorsement or recommendation for use.

DOI: 10.1021/acs.est.5b05059
Environ. Sci. Technol. 2016, 50, 2487−2497

REFERENCES

(1) Pacala, S.; Socolow, R. Stabilization wedges: solving the climate problem for the next 50 years with current technologies. *Science* **2004**, *305*, 968−972.

(2) U.S. Energy Information Adminstration (EIA), *Natural Gas Annual Report*. http://www.eia.gov/naturalgas/annual/pdf/nga11.pdf (accessed February 5, 2016).

(3) Alvarez, R.; Pacala, S.; Winebrake, J.; Chameides, W.; Hamburg, S. Greater focus needed on methane leakage from natural gas infrastructure. *Proc. Natl. Acad. Sci. U. S. A.* **2012**, *109*, 6435−6440.

(4) Wang, Q.; Chen, X.; Jha, A. N.; Rogers, H. Natural gas from shale formation-the evolution, evidences and challenges of shale gas revolution in United States. *Renewable Sustainable Energy Rev.* **2014**, *30*, 1−28.

(5) U.S. Energy Information Adminstration (EIA), *Annual energy outlook 2014*. 2014; http://www.eia.gov/forecasts/aeo/pdf/0383(2014).pdf (accessed February 5, 2016).

(6) Brandt, A. R.; et al. Methane leaks from North American natural gas systems. *Science* **2014**, *343*, 733−735.

(7) Caulton, D. R.; Shepson, P. B.; Santoro, R. L.; Sparks, J. P.; Howarth, R. W.; Ingraffea, A. R.; Cambaliza, M. O.; Sweeney, C.; Karion, A.; Davis, K. J.; Stirm, B. H.; Montzka, S. A.; Miller, B. R. Toward a better understanding and quantification of methane emissions from shale gas development. *Proc. Natl. Acad. Sci. U. S. A.* **2014**, *111*, 6237−6242.

(8) Gentner, D.; et al. Emissions of organic carbon and methane from petroleum and dairy operations in California's San Joaquin Valley. *Atmos. Chem. Phys.* **2014**, *14*, 4955−4978.

(9) Karion, A.; et al. Methane emissions estimate from airborne measurements over a western United States natural gas field. *Geophys. Res. Lett.* **2013**, *40*, 4393−4397.

(10) Karion, A.; et al. Aircraft-based estimate of total methane emissions from the Barnett Shale region. *Environ. Sci. Technol.* **2015**, *49*, 8124−8131.

(11) Allen, D. T.; Torres, V. M.; Thomas, J.; Sullivan, D. W.; Harrison, M.; Hendler, A.; Herndon, S. C.; Kolb, C. E.; Fraser, M. P.; Hill, A. D.; Lamb, B. K.; Miskimins, J.; Sawyer, R. F.; Seinfeld, J. H. Measurements of emissions at natural gas production sites in the United States. *Proc. Natl. Acad. Sci. U. S. A.* **2013**, *110*, 17768−17773.

(12) Marchese, A. J.; Vaughn, T. L.; Zimmerle, D. J.; Martinez, D. M.; Williams, L. L.; Robinson, A. L.; Mitchell, A. L.; Subramanian, R.; Tkacik, D. S.; Roscioli, J. R.; Herndon, S. C. Methane emissions from United States natural gas gathering and processing. *Environ. Sci. Technol.* **2015**, *49*, 10718−10727.

(13) Johnson, D. R.; Covington, A. N.; Clark, N. N. Methane emissions from leak and loss audits of natural gas compressor stations and storage facilities. *Environ. Sci. Technol.* **2015**, *49*, 8132−8138.

(14) Subramanian, R.; Williams, L. L.; Vaughn, T. L.; Zimmerle, D.; Roscioli, J. R.; Herndon, S. C.; Yacovitch, T. I.; Floerchinger, C.; Tkacik, D. S.; Mitchell, A. L.; Sullivan, M. R.; Dallmann, T. R.; Robinson, A. L. Methane emissions from natural gas compressor stations in the transmission and storage sector: Measurements and comparisons with the EPA greenhouse gas reporting program protocol. *Environ. Sci. Technol.* **2015**, *49*, 3252−3261.

(15) Harriss, R.; Alvarez, R. A.; Lyon, D.; Zavala-Araiza, D.; Nelson, D.; Hamburg, S. P. Using Multi-Scale Measurements to Improve Methane Emission Estimates from Oil and Gas Operations in the Barnett Shale Region, Texas. *Environ. Sci. Technol.* **2015**, *49*, 7524−7526.

(16) Lyon, D. R.; Zavala-Araiza, D.; Alvarez, R. A.; Harriss, R.; Palacios, V.; Lan, X.; Talbot, R.; Lavoie, T.; Shepson, P.; Yacovitch, T. I.; Herndon, S. C.; Marchese, A. J.; Zimmerle, D.; Robinson, A. L.; Hamburg, S. P. Constructing a spatially resolved methane emission inventory for the Barnett Shale Region. *Environ. Sci. Technol.* **2015**, *49*, 8147−8157.

(17) Brantley, H.; Thoma, E.; Squier, W.; Guven, B.; Lyon, D. Assessment of Methane Emissions from Oil and Gas Production using Mobile Measurements. *Environ. Sci. Technol.* **2014**, *48*, 14508−14515.

(18) Rella, C. W.; Tsai, T. R.; Botkin, C. G.; Crosson, E. R.; Steele, D. Measuring Emissions from Oil and Natural Gas Well Pads Using the Mobile Flux Plane Technique. *Environ. Sci. Technol.* **2015**, *49*, 4742−4748.

(19) Yacovitch, T. I.; Herndon, S. C.; Pétron, G.; Kofler, J.; Lyon, D.; Zahniser, M. S.; Kolb, C. E. Mobile Laboratory Observations of Methane Emissions in the Barnett Shale Region. *Environ. Sci. Technol.* **2015**, *49*, 7889−7895.

(20) Lan, X.; Talbot, R.; Laine, P.; Torres, A. Characterizing fugitive methane emissions in the Barnett Shale area using a mobile laboratory. *Environ. Sci. Technol.* **2015**, *49*, 8139−8146.

(21) Mitchell, A. L.; Tkacik, D. S.; Roscioli, J. R.; Herndon, S. C.; Yacovitch, T. I.; Martinez, D. M.; Vaughn, T. L.; Williams, L. L.; Sullivan, M. R.; Floerchinger, M.; Omara, C.; Subramanian, R.; Zimmerle, D.; Marchese, A. J.; Robinson, A. L. Measurements of methane emissions from natural gas gathering facilities and processing plants: Measurement results. *Environ. Sci. Technol.* **2015**, *49*, 3219−3227.

(22) Zavala-Araiza, D.; Lyon, D.; Alvarez, R. A.; Palacios, V.; Harriss, R.; Lan, X.; Talbot, R.; Hamburg, S. P. Toward a functional definition of methane super-emitters: Application to natural gas production sites. *Environ. Sci. Technol.* **2015**, *49*, 8167−8174.

(23) Phillips, N. G.; Ackley, R.; Crosson, E. R.; Down, A.; Hutyra, L. R.; Brondfield, M.; Karr, J. D.; Zhao, K.; Jackson, R. B. Mapping urban pipeline leaks: Methane leaks across Boston. *Environ. Pollut.* **2013**, *173*, 1−4.

(24) Jackson, R. B.; Down, A.; Phillips, N. G.; Ackley, R. C.; Cook, C. W.; Plata, D. L.; Zhao, K. Natural gas pipeline leaks across Washington, DC. *Environ. Sci. Technol.* **2014**, *48*, 2051−2058.

(25) U.S. EPA, *Other Test Method (OTM) 33 and 33A Geospatial Measurement of Air Pollution-Remote Emissions Quantification Direct Assessment (GMAP-REQ-DA)*. 2014; http://www.epa.gov/ttn/emc/prelim.html (accessed February 5, 2016).

(26) Foster-Wittig, T. A.; Thoma, E. D.; Albertson, J. D. Estimation of point source fugitive emission rates from a single sensor time series: a conditionally-sampled Gaussian plume reconstruction. *Atmos. Environ.* **2015**, *115*, 101−109.

(27) Gryning, S.; Holtslag, A.; Irwin, J.; Sivertsen, B. Applied dispersion modelling based on meteorological scaling parameters. *Atmos. Environ.* **1987**, *21*, 79−89.

(28) Horst, T.; Weil, J. Footprint estimation for scalar flux measurements in the atmospheric surface layer. *Bound.-Lay. Meteorol.* **1992**, *59*, 279−296.

(29) Van Ulden, A. Simple estimates for vertical diffusion from sources near the ground. *Atmos. Environ.* **1978**, *12*, 2125−2129.

(30) Yee, E.; Flesch, T. Inference of emission rates from multiple sources using Bayesian probability theory. *J. Environ. Monit.* **2010**, *12*, 622−634.

(31) Yee, E. Probability Theory as Logic: Data Assimilation for Multiple Source Reconstruction. *Pure Appl. Geophys.* **2012**, *169*, 499−517.

(32) Chenghui, C.; Ferrari, S. Information-Driven Sensor Path Planning by Approximate Cell Decomposition. *IEEE Trans. Syst. Man Cybern. B Cybern.* **2009**, *39*, 672−689.

(33) Ferrari, S.; Chenghui, C. Information-Driven Search Strategies in the Board Game of CLUE. *IEEE Trans. Syst. Man Cybern. B Cybern.* **2009**, *39*, 607−625.

(34) Zhang, G.; Ferrari, S.; Cai, C. A Comparison of Information Functions and Search Strategies for Sensor Planning in Target Classification. *IEEE Trans. Syst. Man Cybern. B Cybern.* **2012**, *42*, 2−16.

(35) Cover, T.; Thomas, J. *Elements of Information Theory*, Second ed.; Wiley, 2006.

(36) Latombe, J.-C. *Robot Motion Planning*; Kluwer Academic Publishers: Norwell, MA, USA, 1991.

(37) Jensen, F. In *Bayesian Networks and Decision Graphs*; Jordan, M., Lauritzen, S., Lawless, J., Nair, V., Eds.; Statistics for Engineering and Information Science; Springer-Verlag: New York, 2001.

DOI: 10.1021/acs.est.5b05059
Environ. Sci. Technol. 2016, 50, 2487−2497